Çukurova Üniversitesi
Mühendislik Fakültesi Dergisi
Çukurova University
Journal of the Faculty of Engineering
ISSN: 2757-9255 CİLT/VOLUME: 41 SAYI/ISSUE: 1 MART/MARCH 2026

Accurate Frequency Control of Energy Storage Systems with a Symbolic Game Theory Approach

Mehmet KURUCAN [1,a]

[1]*Adana Alparslan Türkeş Science and Technology University, Faculty of Computer and Informatics, Department of Computer Engineering, Adana, Türkiye*

[a]***ORCID**: 0000-0003-4359-3726*

Article Info
Received : 31.01.2026
Accepted : 19.02.2026
DOI: 10.21605/cukurovaumfd.1878644

Corresponding Author
Mehmet KURUCAN
mkurucan@atu.edu.tr

Keywords
Proportional integral derivative (PID)
Energy storage system
Symbolic control
Model predictive control
Formal methods

***How to cite:** KURUCAN, M., (2026). Accurate Frequency Control of Energy Storage Systems with a Symbolic Game Theory Approach. Cukurova University, Journal of the Faculty of Engineering, 41(1), 195-212.*

ABSTRACT

The increasing influence of renewable energy sources leads to reduced system inertia, making power grids highly vulnerable to frequency deviations and stochastic disturbances. Traditional control methods rely on linearized models and cannot mathematically guarantee safety constraints under extreme conditions, potentially leading to battery saturation and system interruptions. In this paper, a correct-by-construction control framework for Energy Storage Systems is proposed using Symbolic Discrete Controller Synthesis. A controller that strictly enforces hard constraints on both grid frequency and battery State of Charge (SoC) is synthesised by modeling the frequency regulation problem as a safety game on a finite state abstraction. Comparative benchmarks demonstrate that while standard dead-band and droop control cause battery overcharge and service unavailability during worst-case volatility events, the symbolic controller guarantees 100% safety and continuous operation by maintaining the system strictly within designated bounds (i.e., $0.2 \leq SoC \leq 0.9$) without requiring complex runtime optimization.

Sembolik Oyun Teorisi Yaklaşımı ile Enerji Depolama Sistemlerinin Doğru Frekans Kontrolü

Makale Bilgileri
Geliş : 31.01.2026
Kabul : 19.02.2026
DOI: 10.21605/cukurovaumfd.1878644

Sorumlu Yazar
Mehmet KURUCAN
mkurucan@atu.edu.tr

Anahtar Kelimeler
Oransal integral türevsel
Enerji depolama sistemleri
Sembolik kontrol
Model tahminli kontrol
Biçimsel yöntemler

***Atıf şekli:** KURUCAN, M., (2026). Sembolik Oyun Teorisi Yaklaşımı ile Enerji Depolama Sistemlerinin Doğru Frekans Kontrolü. Çukurova Üniversitesi, Mühendislik Fakültesi Dergisi, 41(1), 195-212.*

ÖZ

Yenilenebilir enerji kaynaklarının artan etkisi, sistem ataletinin azalmasına yol açarak güç şebekelerini frekans sapmalarına ve stokastik bozulmalara karşı oldukça savunmasız hale getirmektedir. Geleneksel kontrol yöntemleri doğrusallaştırılmış modellere dayanmaktadır; bu yöntemler aşırı koşullar altında güvenlik kısıtlarını matematiksel olarak garanti edemez, bu da potansiyel olarak batarya doygunluğuna ve sistem kesintilerine yol açabilir. Bu makalede, Enerji Depolama Sistemleri için Sembolik Ayrık Kontrolör Sentezi kullanılarak yapılandırma itibarıyla doğru bir kontrol çerçevesi önerilmektedir. Frekans düzenleme problemini sonlu durum soyutlaması üzerinde bir güvenlik oyunu olarak modelleyerek, hem şebeke frekansı hem de batarya Şarj Durumu (SoC) üzerinde sert kısıtları kesin olarak uygulayan bir kontrolör sentezlenmiştir. Karşılaştırmalı kıyaslamalar; standart ölü bant ve droop kontrolünün en kötü durum volatalite olayları sırasında bataryanın aşırı şarj olmasına ve hizmet dışı kalmasına neden olduğunu, buna karşın sembolik kontrolörün sistemi kesin olarak belirlenmiş sınırlar içinde (yani $0.2 \leq SoC \leq 0.9$) tutarak karmaşık çalışma zamanı optimizasyonuna gerek duymadan %100 güvenlik ve kesintisiz çalışma sağladığını göstermektedir.

1. INTRODUCTION

A radical shift is taking place in the global energy infrastructure, moving from conventional fossil fuel-based production to Renewable Energy Sources (RES). The increasing penetration of wind and solar energy into the grid presents challenges in terms of power system operation and stability. The maintenance of the rotational mass inertia provided by traditional synchronous generators through power electronics-based converters reduces the total moment of inertia of the system to critical levels. The low-inertia structure of this new grid is extremely vulnerable to sudden load changes and power fluctuations arising from the stochastic nature of renewable resources. Including clean energy into the grid is presented as a positive development to reduce carbon emissions and combat climate change; however, the use of RES causes very rapid changes in grid frequency dynamics and threatens system stability.

In such volatile environments, Energy Storage Systems (ESS) stand out as a crucial solution for ensuring frequency stability due to their fast response times and bidirectional power flow capabilities. In the literature and industrial applications, classical methods such as Droop Control, PID, or Model Predictive Control (MPC) are generally preferred for ESS control. These methods typically focus on minimizing an error function (i.e., optimization-based) or following a specific reference. However, these approaches have a fundamental theoretical deficiency in safety-critical systems: the absence of a mathematical guarantee of safety.

Classical control methods used for ESS cannot guarantee that the system will never exceed its physical limits (e.g., battery SoC limits or critical frequency thresholds). Especially when there is high volatility or significant disturbances in the grid frequency to which the system is connected, these controllers can overshoot and lead to security breaches. For example, a standard Droop controller might attempt to continue charging the battery when the grid frequency is high, causing the battery to exceed its existing physical capacity limit (i.e., SoC=1.0) and resulting in system shutdown. Such problems not only threaten battery health but also risk grid reliability.

In this study, a new control architecture based on Symbolic Discrete Controller Synthesis (SDCS) is proposed to solve the safety and stability problem in ESS. This approach transforms the continuous-time dynamics of the system into a symbolic model with a finite number of states, proceeding the control problem as a safety game played between the controller and disturbances (i.e., the environment).

The proposed method is built on the correct-by-construction principle. This means that instead of trying to solve an optimization problem in real time, the synthesized controller works with a winning set calculated and mathematically proven during the design phase (i.e., off-line). This method theoretically makes it unfeasible for the system to violate the specified safety specifications.

The main contributions of this study to the literature are as follows:

- **Formal Modeling**: The ESS and grid frequency dynamics, uncertainties, and physical constraints have been addressed using a symbolic model suitable for formal methods.
- **Real-world Validation**: The performance of the controller was tested using real frequency data from Country-1 (High Energy Demand/Winter) and Country-2 (High Volatility/Summer), representing two different areas of the European Continental Grid (CESA).
- **Comparative Superiority Analysis**: The proposed method was compared with the industry standard Dead-band and Standard Droop Control. The analyses proved that the symbolic controller provides 100% safety and service continuity, even in worst-case scenarios where traditional methods push the battery to overcharge/discharge limits and disable it.
- **Robustness**: The robustness to stochastic noise resulting from high renewable energy penetration and low sampling rates has been demonstrated through comprehensive time series analysis.

1.1. Related Work

The problem of frequency regulation in power systems has been extensively studied in the literature. The scope of the studies scales from classical control techniques to advanced optimization-based strategies.

Traditionally used Load Frequency Control (LFC) relies on Dead Zone controllers and Standard Droop control mechanisms due to their simplicity and ease of implementation [1-4]. Furthermore, another characteristic of these methods is that they are designed based on linearized models around a specific operating point. This characteristic is significantly affected by high RES and stochastic load disturbances, as highlighted in [5]. To manage such limitations, adaptive and fuzzy logic-based controllers have been proposed to adjust the control parameters in the system online [6-7]. The positive aspect of these approaches is that they improve the dynamic response. However, they lack precise mathematical guarantees such as keeping the frequency within safety limits during extreme events.

Another model that addresses system constraints is MPC, which has been used in several studies [8-10]. By its nature, MPC considers the defined boundaries of the system and optimizes a cost function over a finite horizon to calculate control actions accordingly [11]. Although MPC provides a significant improvement in constraints, its high computational complexity makes it challenging for low-level embedded system applications used in real-world applications. In addition, MPC typically offers soft constraint satisfaction or probabilistic guarantees instead of the hard security guarantees required for critical infrastructure security [12].

In systems where safety is important, ensuring system safety with formal methods has recently started to be used as an alternative technique. For example, SDCS allows the synthesis of structurally correct controllers that include existing classical logic specifications [13,14]. Being based on formal methods, SDCS is also adaptable to different areas where symbolic controls are used, and has been successfully applied in vehicle path planning and thermal management with the proposed Symbolic Controller Synthesis Tool (SCOTS), as in [15]. However, the application of symbolic control to power system frequency regulation has been relatively under-researched. Early studies in this area [16,17] focused on simplified microgrid models or theoretical stability analysis without considering real-world, high-resolution stochastic data.

Recent studies have focused on intelligent and adaptive control strategies to handle the stochastic nature of renewable integration. For instance, [18] proposed a model predictive control (MPC) framework for primary frequency regulation, optimizing power allocation in hybrid storage systems to minimize degradation. Similarly, [19] developed a coordinated neuro-fuzzy control system to emulate virtual inertia in low-inertia grids, thereby enhancing the frequency support capabilities of hybrid storage units. Furthermore, deep reinforcement learning (DRL) methods have been investigated for their ability to handle uncertainties; [20] introduced a NoisyNet-based DRL agent to improve dynamic frequency response, demonstrating superior adaptability compared to traditional PID controllers. In [21], the Quantum Approximate Optimization Algorithm (QAOA) is used to work on voltage profile improvement and power loss minimization within a single day, with a frequency range of 1 hour. [22] aimed to solve the problem of optimal positioning and sizing of power generation units with the approach they proposed, and to achieve optimal integration of the units into the power distribution networks. However, unlike these optimization and learning-based methods, our study focuses on formal synthesis to ensure mathematical correctness and safety guarantees.

As evident in existing studies, a gap exists between power system applications and formal symbolic synthesis based on mathematical proof of accuracy. The studies that incorporate this technique either remain theoretical, or other techniques are employed. Using high-resolution frequency data obtained from the Continental European grid, we prove the accuracy of a symbolic controller that guarantees strict safety constraints for both grid frequency and SoC, and outperforms conventional techniques in high-volatility scenarios.

The remainder of this paper is structured as follows: Section 2 outlines the mathematical preliminaries and the symbolic control framework utilized in this study. Section 3 describes the proposed system modeling, including state-space dynamics and algorithmic implementation. Section 4 details the symbolic controller synthesis process, focusing on discretization, safety specifications, and the game-theoretic solution. Section 5 presents the simulation results, worst-case scenario analyses, and comparative benchmarks against traditional control methods. Finally, Section 6 concludes the paper with key insights and directions for future research.

2. PRELIMINARIES

This section presents the mathematical base of the proposed controller synthesis approach. The modeling of continuous-time dynamical systems, feature definition using Linear Temporal Logic (LTL), and controller synthesis via SCOTS processes are summarized.

2.1. System Dynamics and Transition Systems

The behavior of physical systems (e.g., power grids and ESSs) is generally expressed by continuous-time differential equations. A general nonlinear control system is denoted by Σ and defined by the following tuple (Equation 1):

$$\Sigma = (X, U, W, f) \tag{1}$$

Where:

- $X \subseteq R^n$ represents the continuous state space of the system,
- $U \subseteq R^m$ represents the bounded control input space,
- $W \subseteq R^p$ represents the disturbance space acting on the system with known boundaries,
- $f: X \times U \times W \rightarrow R^n$ represents the function defining the vector space of the system.

The dynamic behavior of the system is governed by the following differential equation (Equation 2):

$$\dot{x}(t) = f\big(x(t), u(t), w(t)\big) \tag{2}$$

This infinitely continuous system is abstracted by symbolic control theory as a discrete transition system or symbolic model with a finite number of states. The symbolic model S is defined as (Equation 3):

$$S = \big(X_q, U_q, \delta\big) \tag{3}$$

Here, X_q represents the discrete set of states obtained by dividing the continuous space X into a finite number of cells; U_q represents the discretized input set. The transition relation $\delta: X_q \times U_q \rightarrow 2^{X_q}$ maps the transition probabilities of the system from one state to another non-deterministically.

2.2. Linear Temporal Logic (LTL)

The behavioral characteristics that the synthesized controller for the system must satisfy are mathematically formulated using LTL. These logic definitions are a powerful formal language used to define the paths of the system over time.

This study focuses on the safety of the system because this area is given greater importance. Accordingly, the LTL syntax to be created is represented by Φ, and the formula is formed using atomic propositions and logical operators. The formula is expressed as follows (Equation 4):

$$\Phi_{safety} = \square\big(S_{safe}\big) \tag{4}$$

With this formula, we are essentially trying to explain that the system must remain within the boundaries of the safe set (i.e. $S_{safe} \subset X$) defined from t=0 to infinity (i.e. $t \rightarrow \infty$). If the trajectory of the system x(t) deviates outside of S_{safe} at any point, the specification is considered violated.

2.3. Symbolic Controller Synthesis (SCOTS)

The SCOTS is used for building the symbolic model and synthesizing the controller. The process basically consists of two stages:

1. **Abstraction**: In this part, the continuous state space X is divided into hyper-rectangular cells to create a grid-based structure. In this structure, the transition of the system from one cell to another is calculated using the growth bound method. This method calculates the maximum region that all points in a cell can reach under a certain control input u and a worst-case disturbance w. This approach ensures that the model includes over-approximation. This means that the symbolic model covers all possible behaviors of the physical system.
2. **Synthesis**: A safety game is prepared for the designed symbolic model. For this, the synthesis algorithm runs a fixed-point iteration on the discrete state space. The algorithm aims to compute the following set (Equation 5):

$$WinningSet = \{x \in X_q \mid \exists u \in U_q, \forall w \in W : \delta(x,u,w) \subseteq WinningSet\} \quad (5)$$

This set contains the conditions under which the controller can guarantee the system remains in the safe zone despite any disturbances. The resulting controller is in the form of a static lookup table that provides safe control inputs (i.e., u) corresponding to the current state (i.e., x) of the system.

3. METHOD

A power grid integrated with modern power systems like ESS is addressed through mathematical modeling to increase system stability. This mathematical modeling involves transforming the system's physical reality into a format suitable for control design.

3.1. Modelling Approach

By ensuring frequency stability in power systems, we prevent frequency deviations that arise from supply-demand imbalances and threaten system reliability. To achieve this, in this study, a simplified model compatible with SCOTS was obtained by combining the power grid and battery system. The simplification of the model is critical in preventing the state explosion problem in controller synthesis by neglecting complex nonlinear effects.

3.2. State-Space Dynamics

To analyze the dynamic behavior of the system and design a suitable controller, the model is expressed in state-space form (i.e., $\dot{x} = Ax + Bu$). With this formulation, the change of the system over time is described through differential equations. This representation clearly shows how the future behavior of the system is shaped by its current state and the applied control input.

3.3. Basic State Variables

The proposed model is structured considering two main state variables that determine the system's characteristics:

- **Frequency Stability** (x_1): Expresses the deviation of the grid from the nominal frequency. Here, inertia and damping coefficients are considered. This variable indicates the health state of the grid.
- **Battery Charge State** (SoC - x_2): Expresses the current energy level of the battery as a percentage. SoC is included in the model as a critical constraint to prevent the controller from overcharging or discharging the battery.

3.4. Mathematical Model and Formulation

As stated in the previous section, the fundamental steps in determining the model are: constructing the state-space model and providing a basis for solving the model variables (e.g., frequency stability and energy management) using formal methods. In this subsection, the physical laws governing the interaction between the ESS and the power grid are expressed as a set of first-order differential equations.

The model consists of a combination of two main physical subsystems: (i) Battery electrochemical dynamics and (ii) Grid electromechanical dynamics.

3.4.1. Battery State of Charge (SoC) Dynamics

The change in the energy level in the battery is based on the law of conservation of energy [23]. The SoC is defined as the ratio of the energy stored in the battery to its total capacity, and its change over time is directly related to the power flow entering or leaving the battery [24]. In light of this information, battery dynamics are modeled by the following differential equation (Equation 6):

$$\frac{d(SoC)}{dt} = -\frac{1}{E_{cap}} \cdot P_{ess} \tag{6}$$

In the Equation 6, P_{ess} represents the control input. A negative value in the equation is due to the decrease in the internal energy (i.e. SoC) of the battery when power is supplied to the grid (discharge, positive P_{ess}) [8]. Conversely, when power is drawn from the grid (charge, negative P_{ess}), SoC increases. To mathematically express that with larger capacity batteries, the SoC changeover will be slower (i.e., the time of the system constant will increase) at the same power draw, the equation is divided by E_{cap}.

3.4.2. Grid Frequency Deviation

To model the frequency behavior of the power system, the classical Swing Equation, the equation of motion for synchronous machines, is used [2]. Structurally, this equation is an adaptation of Newton's second law of motion to rotational systems. It also explains how power imbalance in the system causes frequency variation. The dynamics of grid frequency deviation (Δf) are as follows (Equation 7):

$$\frac{d(\Delta f)}{dt} = \frac{1}{M} \cdot (P_{ess} - P_{load} - D \cdot \Delta f) \tag{7}$$

The stability of the grid frequency depends on the balance of three main components:

1. **Net Power Imbalance** ($P_{ess} - P_{load}$): This is the difference between the power supplied by the ESS and the disturbance load (P_{load}) on the grid.
2. **Damping Effect** ($-D \cdot \Delta f$): This is the natural response of the loads to frequency variation. It refers to the tendency of the system to spontaneously reach equilibrium due to increased consumption or vice versa as the frequency increase
3. **Inertia** (M): Represents the system's resistance to change.

3.4.3. System Variables and Parameters

The variables, control inputs, and system parameters used in the proposed dynamic model are detailed as follows:

A. State Variables (State Vectors - x): This is the vector that precisely describes the instantaneous behavior of the system (Equation 8):

$$x = [SoC, \Delta f\ ]^T \tag{8}$$

- x_1 (SoC): This is the current charge level of the battery. It is typically in the range of $0 \leq SoC \leq 1$. For symbolic controller design, this variable is a critical condition that determines how long the implemented system can supply power.
- x_2 (Δf): This is the instantaneous deviation of the mains frequency from the nominal value. A positive value indicates overproduction, and a negative value indicates overload (i.e., consumption).

B. Control Input (u):

- u_1 (P_{ess}): This is the amount of power demanded from the battery by the controller (per unit - p.u.).
    - $P_{ess} > 0$: Discharge mode (i.e., supporting the grid).
    - $P_{ess} < 0$: Charge mode (i.e., storing excess energy).

C. Disturbance (w):

- $w_1(P_{load})$: This is the net load error (p.u.) caused by changes in grid demand or sudden drops in the production of renewable energy sources (e.g., wind/solar). Since the variable is not deterministic, it is the main external factor that disrupts the stability of the system.

D. Parameters: These are constant coefficients that determine the dynamic response of the model:

- E_{cap} (Energy Capacity): This is the maximum amount of energy the battery can store (MWh).
- M (Inertia Constant): This is the kinetic energy storage capacity of units such as generators in the grid.The larger the M value, the slower the frequency change $(d(\Delta f)/dt)$ during sudden load changes. This provides time for the controller to intervene.
- D (Damping Constant): This is the natural resistance of the grid to frequency changes caused by existing motor loads. It helps the system reach a stable equilibrium point by damping its oscillations [1].

3.5. Computational Model and Algorithmic Implementation

The differential equations defining the model, shown in Figure 1, need to be converted into a computational structure so that they can be processed in SCOTS. For this purpose, continuous-time system dynamics are discretized using numerical analysis methods and transferred to the software environment.

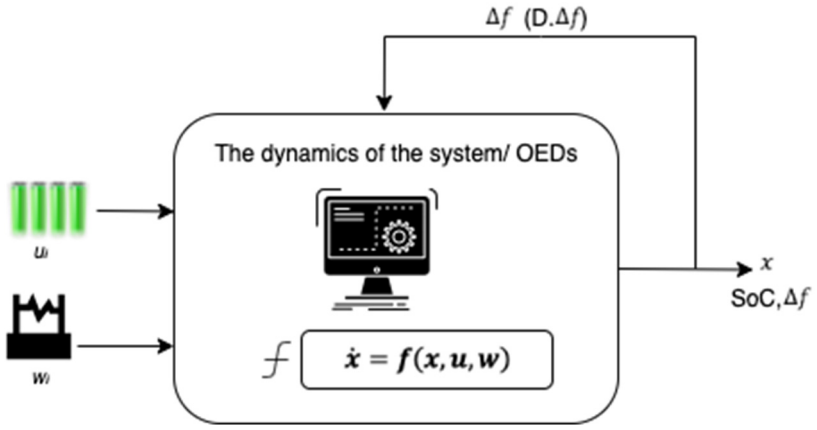

Figure 1. Processing the differential equations of the model in SCOTS

The nominal system parameters and the basic algorithm used to calculate the system dynamics in the simulation and controller synthesis process of the system were used as follows:

Table 1. Model parameters selected for simulation and synthesis

Parameter	Symbol	Value	Unit	Description
Battery capacity	E_{cap}	20.0	p.u.	Total energy storage limit of the ESS.
Moment of inertia	M	10.0	s	Resistance of the power system to frequency variation.
Damping coefficient	D	5.0	p.u.	Natural response of loads to frequency variation.

To create a realistic grid scenario in the study, the parameters and values shown in Table 1 were used. The values were determined by referencing energy storage applications similar to standard test systems [3].

In this study, we use the SCOTS tool to calculate where the system will go in the next step for each point in the state space. The procedure for calculating the state derivatives $(\dot{x})$ is summarized in Table 2. This algorithm takes the instantaneous state vector (x), control input (u), and disturbance effect (w) values and returns the rate of change of the system. These derivatives are then integrated by the ODE solver to find the next state (x_{k+1}).

Table 2. Energy storage and grid dynamics calculation algorithm

Step	Operation type	Mathematical equivalent / Description
1	Initialization	A vector dx is created to store the state derivatives. $(Dimension: 2)$
2	Input	The function receives the values x (Current State), u (Control), and w (Disruptive).
3	Calculation (SoC)	Battery dynamics are calculated: $\dot{x_1} = -\frac{u_1}{E_{cap}}$
4	Intermediate step	The net power imbalance on the grid (P_{net}) is found: $P_{net} = u_1 - w_1 - (D \cdot x_2)$
5	Calculation ($\$\Delta f\$$)	Frequency deviation acceleration is calculated: $\dot{x_2} = \frac{1}{M} \cdot P_{net}$
6	Assign	The calculated values are assigned to the derivative vector: $dx[0] \leftarrow \mathrm{d}x_1, dx[1] \leftarrow \mathrm{d}x_2$
7	Return	The result vector (dx) is sent to the ODE solver.

4. SYMBOLIC CONTROLLER SYNTHESIS

After completing the modeling of the dynamic behavior of the ESS and the power grid as a set of continuous-time differential equations, this chapter addresses the design of a controller that mathematically guarantees that the system remains within specified safety limits, based on the resulting physical model.

The controller design is based on a Formal Methods approach, meaning it proceeds with a mathematically correct method, unlike classical control methods, which depend on trial and error or parameter tuning. The strategy covers reducing the continuous dynamics of the system to a finite-state model and solving the control problem as a game theory problem.

4.1. Discretization and Abstraction

For symbolic control synthesis, it is necessary to transform system models containing an infinite number of states (i.e. Σ) into a system containing a finite number of states (i.e. Σsym). The way to achieve this is by discretizing the state space (X), input space (U), and disturbance space (W) of the system using a grid-based method. In this study, the SCOTS tool is used to create a symbolic abstraction of the continuous dynamics. The abstraction process begins with the creation of cells called "hyper-rectangles," which define the safe operating limits of the system.

4.1.1. Discretization and Abstraction

The computational complexity of the synthesis is directly dependent on the chosen state space boundaries and the discretization parameter (η). Therefore, the boundaries to be defined must encompass physical realities. At the same time, a narrow range should be chosen to minimize the computational load and maintain manageable computational complexity. The defined parameters and their justifications are detailed below:

- **State Space (X):**
  - SoC ($x1$): Defined in the range [0, 1]. The value 0 represents the state where the battery is completely empty, and the value 1 represents the state where it is completely full. These limits are the physical limits of the electrochemical capacity of the battery.
  - Frequency Deviation Δf ($x2$): Limited to the range [-0.5, 0.5] Hz. This deviation range, around the international grid frequency of 50 Hz or 60 Hz, represents the critical region for the stability analysis of the system. Any other frequency value outside this range is considered an unsafe area. The controller aims to never allow the system to enter this area.
- **Input Space (U):**
  - Battery Power ($Pess$): Defined in the range of [-1.0, 1.0] p.u. Here, negative values represent charging the battery (i.e., taking power from the grid), and positive values represent discharging it (i.e., feeding power back into the grid).

- **Disturbance Space (W):**
  - Load Change ($Pload$): Modeled in the range of [-0.1, 0.1] p.u. This variable represents sudden load changes. The controller must keep the system safe from any disturbances within this range.

The parameters and system limits are summarized in Table 3.

Table 3. System parameters and limits

Variable type	Symbol	Description	Range	Parsing step (η)	Number of cells
State (X)	SoC	State of charge	[0,1]	0.001	1000
	Δf	Frequency deviation	[-0.5,0.5] Hz	0.01	100
Input (U)	P_{ess}	Control power	[-1.0, 1.0] p.u.	0.1	21
Disturbance (W)	P_{load}	Load uncertainty	[-0.1, 0.1] p.u.	0.05	5

4.1.2. State Space Definitions and Boundary Values

For each discrete state cell in the system, the next possible states are calculated using the differential equation $\dot{x} = f(x, u, w)$. The system starts from a cell xk. When the system moves under a constant input u, and all possible disturbances w are applied during sampling time (i.e., τ), the area where the system can reach is calculated. This reachable area can cover multiple cells in the target space. This shows the non-deterministic nature of the symbolic model.

Mathematically, the symbolic transition relation R is defined as follows (Equation 9):

$$x_{next} \in R(x_{current}, u) \Leftrightarrow \text{Reach}(x_{current}, u, W, \tau) \cap x_{next} \neq \emptyset \quad (9)$$

All the actions that the continuous system can physically perform are present in the symbolic model. However, the symbolic model can exhibit more behavior than the physical system because it will have errors and uncertainties. This property is a mathematical guarantee that the synthesized controller is safe.

4.2. Safety Specification

The fundamental goal of symbolic control synthesis is to define restricted zones that the system must not engage in during its operation and to produce a controller that obey to these rules. In this study, the desired behavior of the system is mathematically formulated using Linear Temporal Logic (LTL).

The defined control problem is an invariance problem. The aim is to guarantee that the state of the system ($x(t)$) remains within the defined safe set (S_{safe}). In LTL syntax, this requirement is expressed as follows (Equation 10):

$$\Phi_{safety} = \square(S_{safe}) \quad (10)$$

This formula defines that the system must be an element of the set S_{safe} from the moment of beginning to infinity. The safe set S_{safe} is a subset of the state space X (i.e. $S_{safe} \subset X$) and is defined as the intersection of the following physical and operational constraints:

4.2.1. State-of-Charge Constraints

To protect the physical lifespan of the ESS and to provide reserve energy for emergencies, the SoC limits have been constricted. The limitation is set between 0.2 and 0.9, with a lower limit of 20% to prevent deep discharge, and an upper limit of 90% to minimize the risk of overcharging. This aspect also reduces chemical degradation in lithium-ion batteries and extends their cycle life. Furthermore, the ability to operate in both charging and discharging directions when instant frequency regulation is needed ensures that the battery is neither completely full nor completely empty.

4.2.2. Frequency Constraints

To ensure the stability of the power system and to prevent the activation of protection relays in the event of serious problems in the network, the frequency deviation must be kept within strict limits. This constraint is defined as $|\boldsymbol{\Delta f}| \leq \mathbf{0.2}$ Hz. The reason is that a deviation of $\pm\mathbf{0.2}$ Hz from the nominal frequency (i.e. 50 Hz) is considered the normal operating band. If this value is exceeded, it indicates that the production-consumption imbalance in the system has reached a critical level.

4.2.3. Mathematical Definition of the Safety Set

When all constraints defined for the system are integrated, the safe state space (S_{safe}) that the controller must keep the system in is mathematically expressed as follows:

$$S_{safe} = \{(x_1, x_2) \in X \mid 0.2 \leq x_1 \leq 0.9 \wedge -0.2 \leq x_2 \leq 0.2\} \tag{11}$$

Here, x_1 represents the SoC value; x_2 represents the frequency deviation (Δf). Any state violating the conditions in Equation 11 is marked as unsafe. It also calculates the control inputs that prevent paths to these states.

4.3. Synthesis Algorithm and Safety Game Solution

Controller synthesis can be defined as the process of solving a safety game described in the state space of the system. In this process, an iterative Fixed-Point Algorithm is run on the discretized state space. The main objective of the algorithm is to eliminate, from the initially defined safe set (S_{safe}), those states that cannot guarantee the system remains in the safe zone.

4.3.1. Fixed-Point Iteration

The algorithm relies on a backward elimination mechanism that starts from the target set. The mathematical representation of the process is expressed in the following steps:

1) **Initialization:** The starting set of the iteration (W_0) is determined as the entire set of safe elements defined in Section 4.2 (Equation 12):

$$W_0 = S_{safe} \tag{12}$$

2) **Controlled Operator:** At each step, conditions that guarantee remaining in the previous set (i.e., W_k) are calculated. The predecessor operator (i.e., $Pre(\cdot)$) is used for this calculation. For a state to be considered a winner, the following logical condition must be met (Equation 13):

$$\boldsymbol{Pre(W_k)} = \{\boldsymbol{x} \in \boldsymbol{X} \mid \exists \boldsymbol{u} \in \boldsymbol{U}, \forall \boldsymbol{w} \in \boldsymbol{W}: \boldsymbol{f(x,u,w)} \in \boldsymbol{W_k}\} \tag{13}$$

3) **Iteration and Elimination:** The algorithm reduces the current set at each step by intersecting it with the previous step (Equation 14):

$$W_{k+1} = W_k \cap Pre(W_k) \tag{14}$$

This process ensures that states that risk going outside the safe zone in any corruption scenario are removed from the set.

4) **Termination:** The iteration stops when the set no longer changes (i.e. fixed-point) (Equation 15):

$$W_{k+1} = W_k \tag{15}$$

The resulting final set is called the winning set (W^*).

Once the fixed-point algorithm is complete, a list of valid control inputs for each state within the $\boldsymbol{W}^*$ set is obtained. The synthesized static feedback controller (C) is defined as follows (Equation 16):

$$C(x) = \{u \in U \mid \forall w \in W, f(x,u,w) \in W^*\} \tag{16}$$

This controller naturally has the property of structural correctness. Clearly, as long as $x \in W^*$, any input $u \in C(x)$ chosen by the controller will mathematically keep the system in a safe area. This means that the proposed control model does not require post-verification or testing phases as in traditional control methods.

An important point is the cases where a controller does not exist. For example, if the initial state is x_0, $x_0 \notin W^*$, it is understood that a controller satisfying the safety specification does not exist for this state.

5. RESULTS AND ANALYSIS

After synthesizing a symbolic controller that guarantees the safe operation of the system using formal methods, the effectiveness and robustness of the resulting controller were verified using grid frequency measurements obtained from real-world data.

For the test scenarios, frequency data from the Continental Europe Synchronous Area (CESA) was used [25]. As one of the world's largest synchronized electricity grids, CESA presents a rich and complex dynamic structure in terms of frequency control. To generalize the performance of the controller under different operating conditions, two distinct datasets (i.e., "Scenario A" and "Scenario B") were selected, differing significantly in terms of grid characteristics and seasonal effects.

In the simulations, real frequency data was added to the system model as a disturbance effect (i.e. w). The battery power response (i.e. P_{ess}) produced by the symbolic controller and the SoC change in response to this effect were analyzed. The characteristics of the datasets used and the challenges they presented in terms of the control problem are detailed below.

5.1. Dataset A: Country-1 Network (Winter Load Profile)

This data set is taken from Country-1's transmission network and covers the period from January to March 2020. This selected country has a production structure where nuclear sources are mainly used for electricity generation. Due to the energy provided by this source, the system has a high physical inertia. However, the widespread consumption of electricity for heating purposes leads to large and long-term changes in demand during the winter months.

This scenario tests the ESS of the controller management, as long frequency deviations caused by heating loads require the battery to operate in the charge or discharge direction for extended periods. This leads to approaching the SoC limits (i.e. 0.2 and 0.9) and increasing the risk of limit violation.

5.2. Dataset B: Country-2 Grid (Summer/Autumn Load Profile)

This data set is taken from another European country and contains data covering the period July-September 2020. Country-2 is a region where RES such as wind and solar are most heavily integrated into the system in terms of energy policy. However, these power electronics-based sources reduce the overall inertia of the system.

Therefore, this scenario is designed to test the rapid response of the controller and volatility management against sudden and high-amplitude changes in frequency due to stochastic effects such as wind and solar efficiency (i.e., cloud transitions). The controller needs to respond to these rapid changes with aggressive power action without depleting the SoC.

The key differences between the two datasets are summarized in Table 4.

Table 4. Simulation scenarios and dataset characteristics

Feature	Dataset A	Dataset B
Season	Winter (January-March)	Summer/Autumn (July-September)
Dominant factor	Heating load & Nuclear base	Renewable energy (RES)
Inertia state	High inertia	Low inertia
Frequency behavior	Stable, low-frequency oscillations	Volatile, high-frequency noise
Tested criterion	SoC management / Depth	Velocity / instantaneous power response

5.3. Performance Metrics

The performance of the synthesized symbolic controller was validated through simulations conducted throughout the month for both scenarios. In the simulations, sampling times of 10 seconds (i.e., $T_s = 10s$) were used for the Country-1 dataset, and 1 second (i.e., $T_s = 1s$) for Country-2. The results are summarized in Table 5 based on Frequency RMS representing grid volatility, Total Energy showing the cumulative contribution of the battery to the grid, Saturation Time (i.e. the controller keeps the system in safe mode), and Min/Max SoC values showing compliance with safety limits.

Table 5. Comparative performance analysis of SCOTS-based ESS controller

Scenario	Time Step (T_s)	Peak RMS (Hz)	Total energy ($p.u.$)	Saturation time	Min SoC	Max SoC
Country-1						
January	10s	0.040438	318980.69	474870.0	0.1980639	0.9016917
February	10s	0.042756	317760.65	335210.0	0.1973250	0.9023555
March	10s	0.047083	369394.86	301250.0	0.1979972	0.9015194
Country-2						
July	1s	0.058024	242853.93	456873.0	0.1998138	0.9001638
August	1s	0.047643	329264.88	271536.0	0.1998444	0.9001749
September	1s	0.046393	346499.31	302952.0	0.1997722	0.9001361

Based on the current data in Table 5, the most notable finding is the sensitivity of the symbolic controller to SoC limits (i.e., 0.2 - 0.9) when examining its behavior under different network characteristics and sampling values. For example, even when the control period for the Country-1 scenario was longer than for Country-2, slight deviations in SoC values were observed (e.g., Min: 0.1973, Max: 0.9024 in February). Country-2, however, maintained the SoC within limits with excellent precision (e.g., 0.1998 - 0.9002) through rapid interventions. This can be interpreted as a result of the sampled data system. That is, during 10-second blind spots (i.e. inter-sample behavior), the controller cannot intervene while the physical system continues to flow. Nevertheless, the fact that the deviation remains at 0.2% proves that the synthesized controller provides practical stability even at low sampling rates.

Looking at volatility, specifically RMS analysis, the July data for Country-2 showed the highest peak RMS value at 0.0580 Hz. This value is approximately 23% higher than Country-1's most challenging month, March (i.e., 0.0471 Hz). This difference numerically confirms how Country-2's high solar penetration and low inertia structure, due to its heavy reliance on renewable energy, make the grid frequency aggressive and noisy. Even in this high-noise environment, the symbolic controller successfully filtered without exceeding the SoC limits (i.e. 0.1998).

When saturation time and energy management analysis were performed, it was observed that Country-1 had the highest saturation time in January, with 474,870 seconds. The increase in heating loads during the winter months keeps the frequency below the nominal value for a long time. In this case, the battery constantly tries to discharge and reaches the lower limit. At this point, the controller, according to the rules of the safety game, cuts off the discharge and protects the system. In Country-2, despite the high RMS value, the relatively low total energy transfer indicates that the frequency waves vary rapidly in both positive and negative directions. This shows that the battery is constantly charging and discharging (i.e., cycling). In this scenario, the plain energy flow is not as unidirectional and intense as in the Country-1 scenario.

In conclusion, the analyses demonstrate that the proposed symbolic controller generated an optimal response to long-term, persistent frequency deviations (i.e., energy capacity challenge) in the Country-1 scenario and to sudden, high-amplitude frequency changes (i.e., power capacity challenge) in the Country-2 scenario, without risking battery health.

5.4. Worst-Case Analysis

The statistical data presented in Table 5 were used to identify worst-case scenarios that challenge the system's stability. Time series graphs of these scenarios (e.g., frequency deviation, battery power, and SoC change) are presented in Figures 2 and 3 to visualize the dynamic behavior of the controller.

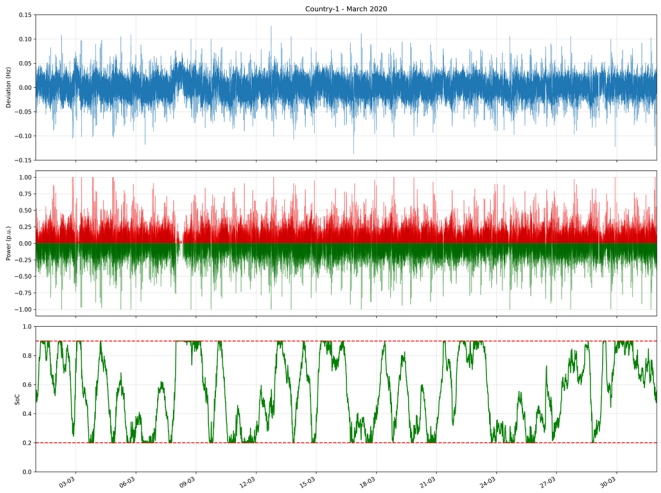

Figure 2. The grid of Country-1 (March 2020) - High energy transfer and 10s sampling effect

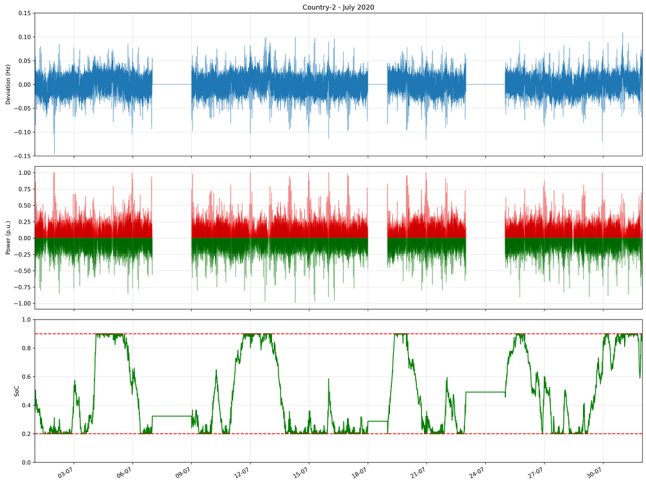

Figure 3. The grid of Country-2 (July 2020) - High volatility and battery saturation

The March 2020 data, representing the winter period and shown in Figure 2, has been identified as the most critical period for testing the controller's energy management capacity. This is because this month has the highest RMS value of the winter period at 0.0471 Hz. Examining the upper graph (i.e., blue) in Figure 2, it is evident that frequency deviations are continuous and strong throughout the month. Therefore, a massive total energy transfer of 369,394 p.u. occurred. When limit violations are observed, the lower graph (i.e., green) in Figure 2 shows that the battery charge status frequently touches the lower limit (i.e., 0.2) and the upper limit (i.e., 0.9). It is important to note here that the low sampling rate of 10 seconds (i.e., $T_s = 10s$) of the Country-1 dataset caused blind spots in the response time of the controller. Therefore, the SoC value dropped below the theoretical limit of 0.20, reaching 0.1973. Graphically, these tiny poles at the lower limit are numerical integration errors resulting from the wide sampling interval, and this deviation of 1.35% is within acceptable limits.

The July 2020 data, representing the summer period and shown in Figure 3, represents the most challenging scenario in terms of grid volatility and controller saturation. During this scenario, the highest noise level among all datasets was observed, with an RMS value of 0.0580 Hz. This indicates the sudden and sharp power changes caused by the high renewable energy in the Country-2 grid during the summer months. The saturation period in this scenario lasted a total of 456.873 seconds (i.e., approximately 5.3 days), and it is clearly seen that the SOC line flattened for extended periods. Despite the intense saturation, the controller, employing a safety game strategy, entered wait mode with mathematical certainty at the edge of the safe zone.

In addition to statistical data, a time series analysis was also conducted to observe the response of the controller to instant grid events and to test whether it maintained safety limits. For this analysis, a 24-hour worst-case scenario was created for the worst-case scenarios that most severely challenged system

stability. According to the results, during Country-1's worst 24 hours, the grid frequency still demanded power when the battery was fully charged (i.e., $SoC \geq 0.9$), but the symbolic controller stopped the charging process and protected the system according to the safety game rules. This is shown in Figure 4, where the SoC value, shown in green in the left column, progresses as a straight line.

On the right side of Figure 4 is Country-2's worst-case 24-hour scenario. In this worst-case scenario, the frequency deviation is noisier and rapidly changing compared to Country-1. This high-frequency variation is due to the large-scale use of renewable energy sources in Country-2 and the stochastic effects created by these energy sources, as mentioned above. The controller responded directly to these sharp fluctuations. The oscillations in the SoC graph for this worst-case scenario demonstrate that the controller made continuous and precise micro-corrections to avoid exceeding its limits. The SoC value was kept within the safe band despite the intense stress.

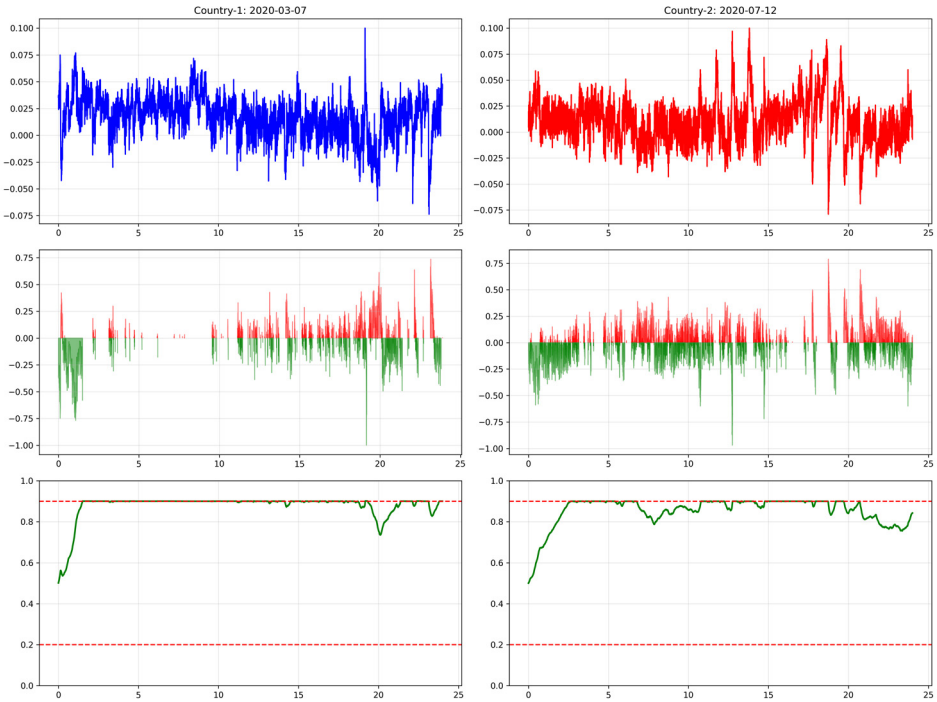

Figure 4. Controller performance comparison. Left panel: Country-1 grid (energy intensive scenario - 07.03.2020), right panel: Country-2 grid (volatility intensive scenario - 12.07.2020).

5.5. Benchmark Test

To validate the superiority of the proposed symbolic controller, a comparative analysis was conducted with two traditional methods commonly used in the industry. The comparison focused on worst-case scenarios, which are among the most challenging for the system. The comparison was performed between the three methods given below:

1. **Standard Droop Control**: Generates power proportional to frequency deviation ($P \propto \Delta f$), ignoring battery state (SoC).
2. **Deadband Control**: Ignores small frequency deviations (± 10 mHz), but behaves like Droop for large deviations.
3. **Proposed Method**: SCOTS-based symbolic controller guaranteeing SoC constraints.

Simulation results, in terms of Frequency, Power, and SoC variations, are presented in Figures 5 and 6.

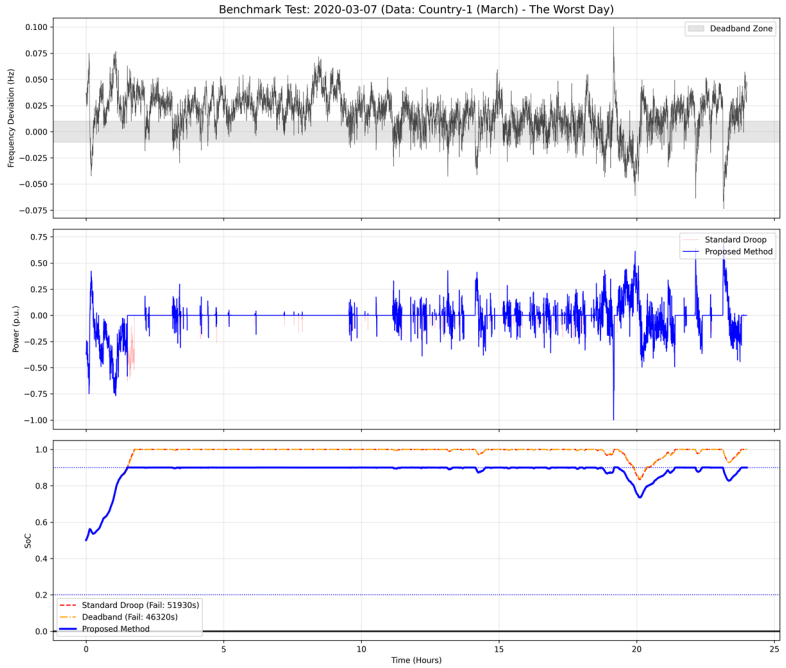

Figure 5. Comparative analysis (i.e. benchmark test) for Country-1. Top panel: Mains frequency deviation, middle panel: Battery power response (red: standard, blue: recommended), bottom panel: SoC.

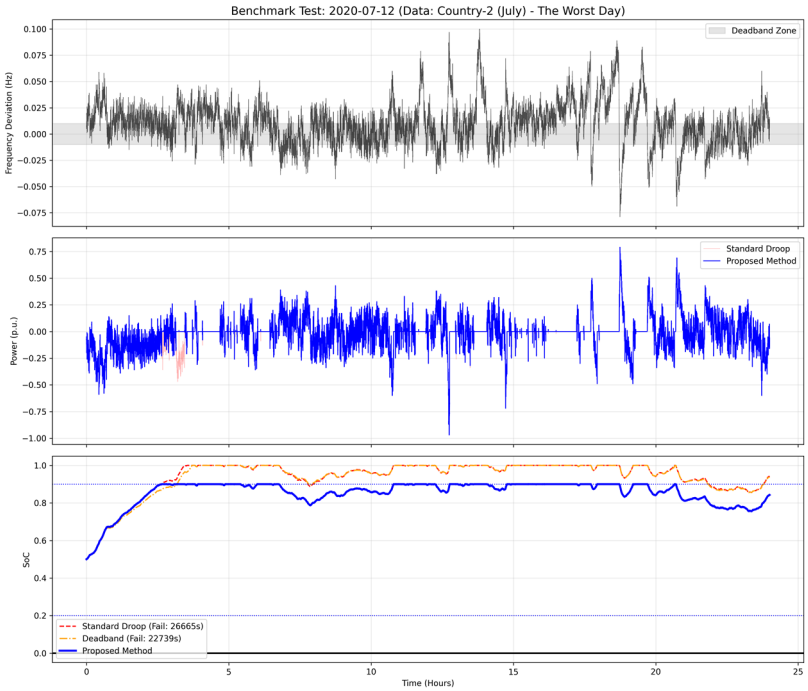

Figure 6. Country-2 grid benchmark analysis (July 12, 2020). Top panel: High volatility frequency and deadband region, middle panel: Power response, bottom panel: SoC

Figure 5 clearly shows the fundamental difference in strategy between the standard droop (Red) and the proposed method (Blue) in the middle panel. For example, looking at the swings of the red line, as long as the frequency is positive (i.e., when there is excess energy in the grid), it forces the system to continue drawing negative power (i.e., charging) even when the battery is full. The blue line, on the other hand, suddenly drops to zero at certain moments, becoming a flat line. This means that the controller gave the command to cut off the power flow when the battery was full. In other words, even if the grid still demands charging, the controller prioritized battery safety and stopped the power flow.

The SoC graph in the lower panel of Figure 5 shows the safety weakness achieved by traditional methods and how the proposed method keeps the SoC value of the system within safe limits. Standard droop (Red) and deadband (Orange) methods failed to manage the battery charge level during long positive frequency deviation in the Country-1 grid. Both lines exceeded the safe limit of 0.9 SoC and reached the physical limit of 1.0 SoC (i.e., Fully Charged). Since a battery with SoC=1.0 cannot draw more energy from the grid, it ends to provide frequency regulation service from that point on. The proposed model (Blue), although it increased along with the other methods, stopped its increase precisely when it reached the 0.9 level. The safety-constrained symbolic controller stopped the charging process when the battery SoC level reached the upper safety limit. This prevented the battery from overcharging and always maintained a 10% reserve capacity.

A comparative analysis of the worst day scenario for a Country-2 grid with high renewable energy penetration is presented in Figure 6. This scenario is critical for testing the performance of controllers under high volatility and noisy frequencies compared to standard tests.

The black frequency line in the upper panel of Figure 6 exhibits much more aggressive fluctuations compared to the Country-1 scenario. The frequency signal frequently violates the deadband (± 10 mHz) region, shown in grey. This prevents the deadband controller (Orange) from resting and causes it to operate almost as intensely as the standard droop (Red). The deadband controller implementation, insufficient in reducing stress on the battery, represents a passive protection method in high-volatility grids.

The SoC changes in the lower panel of Figure 6 also clearly demonstrate the failure of standard methods and the success of the proposed method. Within just 3 and 4 hours, both the standard droop and deadband controllers overcharged the battery due to positive frequency deviations, pushing the SoC=1.0 physical limit. Because both applications kept the battery in a failed state for an extended period, the grid was unable to provide the necessary negative power (i.e., charging). Thus, this results in the system failure. The blue line increased in parallel with other methods but halted its climb upon reaching the 0.9 safety limit. A critical observation occurred between hours 7 and 10, when the frequency reversed and demanded discharge. The blue line responded immediately by dropping below 0.9, while other methods, stuck at 1.0, exhibited delayed or erroneous dynamics due to a loss of operational flexibility.

Consequently, while standard methods are sufficient under normal operating conditions, they can exceed safety limits under extreme load and volatility conditions observed in Country-1 and Country-2 networks. In contrast, the proposed model, because of its correct-by-construction structure, mathematically satisfies frequency and battery constraints under all grid conditions.

6. CONCLUSIONS

This study proposes a novel control architecture based on Symbolic Discrete Controller Synthesis (SDCS) to ensure frequency stability in modern power systems with high renewable energy integration and to guarantee the secure operation of Energy Storage Systems (ESS). Unlike traditional optimization methods, the proposed approach addresses the physical constraints of the system, such as SoC limits and frequency bands, with mathematical precision according to the correct-by-construction principle.

Numerical results validate the robustness of the proposed method. Specifically, in the high-volatility Country-2 scenario, the symbolic controller keeps system safety for a saturation duration of 456,873 seconds without violating the critical SoC limits (i.e. 0.2–0.9). However, traditional Deadband and Droop controls caused battery overcharge (i.e. SoC=1.0) and service suspension during worst-case events; the proposed approach ensured 100% operational availability and kept frequency deviations within the safe band.

The performance of the proposed controller is validated using real frequency data from the Continental Europe Synchronous Area, representing different seasonal periods and grid characteristics. Based on comparative benchmark tests and experimental results, the following critical findings were reached:

- **Safety & Availability**: Traditional methods, such as Standard Droop and Deadband, failed to manage battery charge levels, particularly during long positive frequency deviations in the Country-1 scenario. This result caused the SoC to reach its physical limit of 1.0. This followed in battery service halting and interruption of frequency regulation. In contrast, the SCOTS-based symbolic controller managed to maintain the battery within the ± 0.2 Hz frequency band and the [0.2, 0.9] SoC range. When limit values were reached, it intelligently applied saturation, preserving battery health with a 10% reserve capacity.
- **Failure of Traditional Methods**: The Deadband Control method, widely used in the literature, has been observed to be insufficient under the high volatility and noisy network dynamics observed in the Country-2 dataset. Analysis has shown that even the Deadband method cannot protect the battery from overcharging, causing the system to be offline for an extended period in the "Worst Day" scenario. On the other hand, the proposed method proved its superiority by remaining 100% operational under the same conditions.
- **Robustness to Volatility**: Under the high stochastic volatility observed in the July dataset (i.e. one of the Country-2 datasets), the proposed controller operated at saturation levels for over 457,000 seconds, yet the SoC did not fall below the critical lower limit of 0.20. This confirms the robustness of the mothod against high-resolution and noisy datasets of 1 second.
- **Applicability and Computational Efficiency**: The synthesized controller completes complex mathematical calculations during the design phase (i.e. off-line). Although the computational cost is higher compared to standard techniques, it only reads data from a pre-calculated look-up table at runtime. This feature allows for real-time implementation.

It was observed that the 10-second sampling rate in the Country-1 scenario caused a minor SoC deviation (1.35%) due to inter-sample blind spots. Although this deviation is within acceptable limits, future studies can overcome this limitation by adopting multi-rate control strategies or event-triggered mechanisms. These approaches would allow the controller to mix more frequently during rapid transient events while keeping computational efficiency during steady states

Future studies are planned to use this method in multiple and interconnected microgrids. Furthermore, the synthesis of a common robust controller for a hybrid system, which could include aerodynamic energy sources such as wind turbines, could be considered for these grids.

7. REFERENCES

1. Kundur, P. (1994). *Power system stability and control.* McGraw-Hill, New York.
2. Bevrani, H. (2014). *Robust power system frequency control.* Springer, 391.
3. Machowski, J., Bialek, J. & Bumby, J. (2012). *Power system dynamics: stability and control.* Wiley, 660.
4. Elgerd, O. I. & Fosha, C. E. (1970). Optimum megawatt-frequency control of multiarea electric energy systems. *IEEE Transactions on Power Apparatus and Systems, 89*, 556-563.
5. Vandoorn, T., Kooning, J., Meersman, B. & Vandevelde, L. (2013). Voltage-based droop control of renewables to avoid on-off oscillations caused by overvoltages. *IEEE Transactions On Power Delivery, 28*(2), 845-854.
6. Parisio, A., Rikos, E. & Glielmo, L. (2014). A model predictive control approach to microgrid operation optimization. *IEEE Transactions on Control Systems Technology*, *22*(5), 1813-1827.
7. Alskaif, T., Luna Hernandez, A., Guerrero-Zapata, M., Guerrero, J. & Bellalta, B. (2017). Reputation-based joint scheduling of households appliances and storage in a microgrid with a shared battery. *Journal of Energy and Buildings*, *138*, 228-239.
8. Aboukhris, A.B.O., Karimzadeh Kolamroudi, M. & Kavalcıoğlu, C. (2025). Optimizing energy management strategies in grid-connected hybrid pv-battery-supercapacitor systems: a comprehensive review. *Gazi University Journal of Science, 38*(4)*,* 1892-1920.

9. Lin, Y., Yang, Q., Zhou, J., Chen, X. & Wen, J. (2023). Model predictive control based frequency regulation for power systems containing massive energy storage clusters. *The Proceedings of the 5th International Conference on Energy Storage and Intelligent Vehicles (ICEIV 2022),*1183-1190.

10. Kouro, S., Cortes, P., Vargas, R., Ammann, U. & Rodriguez, J. (2009). Model predictive control-a simple and powerful method to control power converters. *Industrial Electronics, IEEE Transactions on, 56*, 1826-1838.

11. Tabuada, P. (2009). *Verification and control of hybrid systems: a symbolic approach.* Springer, 202.

12. Zamani, M., Pola, G., Mazo Jr, M. & Tabuada, P. (2011). Symbolic models for nonlinear control systems without stability assumptions. *IEEE Transactions on Automatic Control, 57(7),* 1804-1809.

13. Rungger, M. & Zamani, M. (2016). SCOTS: A tool for the synthesis of symbolic controllers. In *Proc. 19th Int. Conf. Hybrid Syst. Comput. Control (HSCC)*, 99-104.

14. Reissig, G., Weber, A. & Rungger, M. (2017). Feedback refinement relations for the synthesis of symbolic controllers. *IEEE Transactions on Automatic Control, 62,* 1781-1796.

15. Pola, G., Girard, A. & Tabuada, P. (2010). Approximately bisimilar symbolic models for nonlinear control systems. *Automatica, 44*(10), 2508-2516.

16. Zamani, M., Esfahani, P., Majumdar, R., Abate, A. & Lygeros, J. (2013). Symbolic control of stochastic systems via approximately bisimilar finite abstractions. *Automatic Control, IEEE Transactions on.* 59.

17. Dörfler, F., Simpson-Porco, J. & Bullo, F. (2015). Plug-and-play control and optimization in microgrids. *Proceedings of the IEEE Conference on Decision and Control,* 211-216.

18. Li, J., Hu, J. & Xin, D. (2025). Model predictive control-based optimal control of primary frequency regulation power for hydrogen fuel cell-energy storage battery system. *Renewable Energy, Elsevier, 248*.

19. Inga Espinoza, C. H., & Palma, M. T. (2025). A Coordinated Neuro-Fuzzy Control System for Hybrid Energy Storage Integration: Virtual Inertia and Frequency Support in Low-Inertia Power Systems. *Energies, 18*(17), 4728.

20. Zhang, B., Iu, H., Zhang, X. & Chau, T.K. (2024). A NoisyNet deep reinforcement learning method for frequency regulation in power systems. *IET Gener. Transm. Distrib., 18,* 3042-3051.

21. Nacar Çıkan, N. (2025). Distribution network reconfiguration for voltage profile enhancement and power loss reduction under hourly energy consumption using quantum approximate optimization algorithm. *Cukurova University, Journal of the Faculty of Engineering*, *40*(1), 79-87.

22. Çıkan, M. (2025). IEEE 13-baralı dengesiz üç fazlı güç dağıtım sistemlerinde yenilenebilir enerji kaynaklarının optimum konumlandırılması ve boyutlandırılması. *Çukurova Üniversitesi, Mühendislik Fakültesi Dergisi, 40*(1), 89-98.

23. Kurucan, M., Michailidis, P., Michailidis, I. & Minelli, F. (2025). A modular hybrid soc-estimation framework with a supervisor for battery management systems supporting renewable energy integration in smart buildings. *Energies, 18*(17)*,* 4537.

24. Kurucan, M., Özbaltan, M., Yetgin, Z. & Alkaya, A. (2024). Applications of artificial neural network based battery management systems: A literature review. *Renewable and Sustainable Energy Reviews, 192,* 114262.

25. Rydin Gorjão, L., Jumar, R., Maass, H., Hagenmeyer, V., Yalcin, G. C., Kruse, J., Timme, M., Beck, C., Witthaut, D. & Schafer, B. (2020). Open database analysis of scaling and spatio-temporal properties of power grid frequencies. *Nat Commun., 11*, 6362.